Burning properties of redox crystals of ammonium nitrate and saccharides

Oluwoye, Ibukun; Altarawneh, Mohammednoor; Dlugogorski, Bogdan

Published in:
Combustion and Flame

DOI:
10.1016/j.combustflame.2019.11.030

Published: 01/03/2020

Document Version
Publisher's PDF, also known as Version of record

Combustion and Flame 213 (2020) 132–139

Contents lists available at ScienceDirect

Combustion and Flame

journal homepage: www.elsevier.com/locate/combustflame

Burning properties of redox crystals of ammonium nitrate and saccharides

Ibukun Oluwoye[a], Mohammednoor Altarawneh[b], Jeff Gore[c], Bogdan Z. Dlugogorski[d,*]

[a] Discipline of Chemistry and Physics, College of Science, Health, Engineering and Education, Murdoch University, 90 South Street, Murdoch, WA 6150, Australia
[b] Chemical and Petroleum Engineering Department, United Arab Emirates University, Sheikh Khalifa bin Zayed St, Al-Ain 15551, United Arab Emirates
[c] Dyno Nobel Asia Pacific Pty Ltd, Mt Thorley, NSW 2330, Australia
[d] Office of Deputy Vice-Chancellor, Research and Innovation, Charles Darwin University, Ellengowan Drive, Darwin, NT 0909, Australia

ARTICLE INFO

Article history:
Received 5 August 2019
Revised 11 October 2019
Accepted 19 November 2019

Keywords:
Monofuels
Explosives
Burning rate
Kinetics
Pollution
NO_x

ABSTRACT

Ammonium nitrate (AN, NH_4NO_3) constitutes the key ingredient of monofuels and civilian-grade explosives, attracting scientific interests aimed at improving their operational and safety performance. This study investigates the combustion properties of redox crystals comprising ammonium nitrate and simple saccharides, with the infrared spectroscopy, X-ray diffraction and molecular modelling. Furthermore, the thermogravimetric measurements afford the isoconversional analysis that yields the overall activation energies of the decomposition process. In addition, the synthesised samples are subjected to elemental and sorption analyses. The results outline (i) the molecular inclusion of the solid fuels within the lattice clusters of AN, (ii) a comparable hygroscopicity behaviour, i.e., a minor increase in affinity towards the absorption of moisture, and (iii) an energetically improved decomposition (and regression) rate, relatively to pristine AN. These features manifest themselves in lower activation energies of redox crystals that enhance the deflagrating properties of these materials for possible application in aviation propellants, and minimise the environmental footprint, especially the emission of nitrogen oxide to the atmosphere, which arises because of inhomogeneities in AN-fuel mixtures commonly used in civilian explosives.

1. Introduction

Ammonium nitrate (AN, NH_4NO_3) remains an essential chemical commodity that serves many industries, including the agricultural and explosive sectors. Civilian and military applications deploy AN as an oxidiser in emulsion (and bulk) explosives, as well as in some propellants and pyrolants. These products are crucial to the sustenance of mining and infrastructure activities [1,2], gas generation mechanisms (e.g., in automotive inflator systems and heavy-lift launchers) [3,4], alternative-fuel engines [5,6], as well as propulsive functions of rockets, satellites and cruise missiles. Although the use of AN continually replaces other conventional oxidisers such as ammonium perchlorates (AP) due to its relatively low cost and halogen-free combustion products, some technical drawbacks have been attributed to the logistics and application of AN in propellants and explosives [7].

The major downsides of AN include (i) its low-temperature transitions and high hygroscopicity which complicate the handling and shelf-life, (ii) its low-burning rate and energetics which influence the performance, mainly as aviation propellants, and (iii) its formation of nitrogen oxides (NO_x, as combustion product) which contributes to atmospheric pollution [1,8]. In fact, the decomposition chemistry of AN is not as “smokeless” as it has been tacitly assumed. The deflagration of solid AN may produce NO_x (an orange plume), propagating initially both by ionic and radical mechanisms in the condensed medium [9,10], and subsequently in the gas-phase reactions [11,12] depending on the temperature, pressure, and confinement [1].

Recent developments focus on enhancing the performance, while maintaining an optimum mechanical and physicochemical properties for prolonged lifespan and negligible environmental impacts [13,14]. These kinds of “modern” high-energy materials require chemical synthesis, modification of existing formulations, or synergistic combinations of various compounds [15–17]. Pertaining to AN, the current advances in the field have resulted in the development of phase-stabilised ammonium nitrate (PSAN), incorporating organic and inorganic modifiers into the crystal lattice

* Corresponding author.
E-mail address: bogdan.dlugogorski@cdu.edu.au (B.Z. Dlugogorski).

https://doi.org/10.1016/j.combustflame.2019.11.030

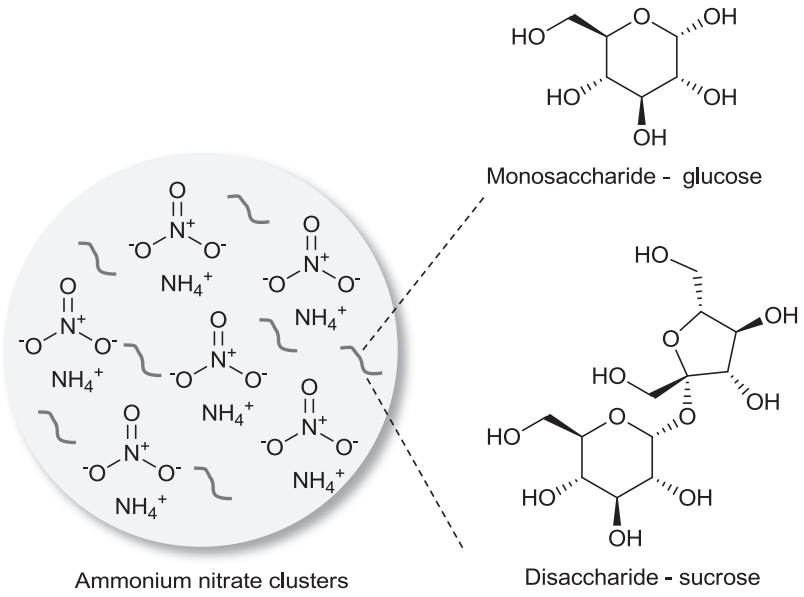

Fig. 1. Planar illustration of saccharides within AN clusters.

of AN [13,18]. In this article, we denote these materials as redox crystals, as they possess both reduction and oxidation capacity in their crystalline make-up. Various metal salts, alkali metal salts, diamine complexes of transition metals, crown ethers, polymers, etc., have been investigated as a potential modifier in PSAN [2,13], serving to eliminate the crystallographic transformation of AN from phase VI to III. The IV ⇌ III phase inversion transpires at ambient temperature, resulting in the formation of undesirable cracks in the propellant grains due to repeated cycles of volume changes (i.e., contraction and expansion of the lattice structure) of about 3.8% [13]. Moreover, the molecular inclusion of some organic substances can both stabilise [19–21] and/or influence the burning behaviour [22] of redox crystals. Mousaviaza et al. [22] demonstrated the latter through the application of polymer binders derived from cellulose as a result of the combustion chemistry of AN and carbon fuel [1].

This work sources inexpensive solid carbohydrates capable of co-crystallising with AN at conditions currently employed in ammonium nitrate plants. Glucose ($C_6H_{12}O_6$) and sucrose ($C_{12}H_{22}O_{11}$) are highly soluble in nonaggressive solvent (i.e., water), have fast crystallisation kinetics, and melting points somewhat close to that of pure AN. Therefore, to surmount the low reactivity and low energetics of AN, we co-recrystallise AN with the two saccharides, to form redox crystals. We hypothesise that, the molecular inclusion of these solid fuels (see Fig. 1) should improve the performance of AN. The experimental observations characterise the molecular structure, carbon and oxygen contents, hygroscopicity, thermal stability, as well as the burning rate. We make relevant remarks pertaining to the handling safety, storage and energetic performance of these redox crystals.

2. Experimental methods

2.1. Material synthesis

In preparation of the samples, we screened out aggressive chemicals as solvents, and focused on identifying crystalline organic compounds, with considerable solubility in water, as source of carbon. This approach elucidated simple saccharides (i.e., glucose and sucrose) as excellent candidates. These carbohydrates have high calorific values (i.e., high heating value, HHV of 15.6 MJ/kg for glucose and 16.5 MJ/kg for sucrose), and yield energetic formulations with good technical properties, e.g., as an explosive [23–26]. Furthermore, glucose and sucrose satisfy molecular requirements [20] of potential "organic modifiers" of AN; they can be characterised as both electron acceptors (due to the presence of an electron withdrawing carbonyl group), and good electron donors (because of the presence of the hydroxyl oxygen). We examined the electrostatic potentials (as well as the molecular orbital gaps) of the selected saccharides as computed by the density functional theory (DFT-D), using the generalised gradient approximation (GGA) exchange-correlation potential of the Perdew–Burke–Ernzerhof (PBE) functional, double numerical plus polarisation (DNP), and Tkatchenko and Scheffler's semiempirical dispersion correction scheme of DMol^3 simulation package [27–29]. A previous study has shown that, the PBE functional performed accurately for high-energy materials [30]. Based on the HOMO–LUMO gaps (i.e., −0.207 for glucose, and −0.181 for sucrose), and the electrostatic potential depicted in Fig. 2, one expects a dipole–dipole attraction (i.e., the formation of hydrogen bonds) as the intermolecular interactions in the AN-saccharide systems. The Supplementary Material contains the Cartesian coordinates of optimised structures of AN and the saccharides.

Since oxygen content plays a crucial role in the formulation of high-energy substances, we expressed oxygen-balance of AN-saccharide redox crystals in terms of their molecular weight (*MW*) and elemental composition, as illustrated in the following equation [31]:

$$\mathrm{OB} = \frac{16\left(\mathrm{O} - 2\mathrm{C} - \frac{1}{2}\mathrm{H}\right)}{\mathrm{MW}} \quad (1)$$

Consequently, ammonium nitrate has an oxygen balance (OB) of +0.20, while the calculated values for glucose (GLU) and sucrose (SU) correspond to −1.07 and −1.12, respectively. Considering an OB of zero, a balanced AN-GLU formulation contains 84.2% AN and 15.8% glucose, while an optimised AN-SU material comprises 84.9% AN and 15.1% sucrose. Hence, the "oxygen balance" (i.e., the fuel mass percent of ~15%), rather than the "crystallographic stoichiometry", guided us in choosing the maximum fraction of these fuels in the synthesised formulations.

During synthesis, we employed each chemical as received from the suppliers; AN (Sigma-Aldrich, ≥99.5%), anhydrous D-glucose (Chem-Supply, analytical reagent), and sucrose (Ajax Finechem, analytical reagent). We dissolved a total of 5.0 g of AN and glucose

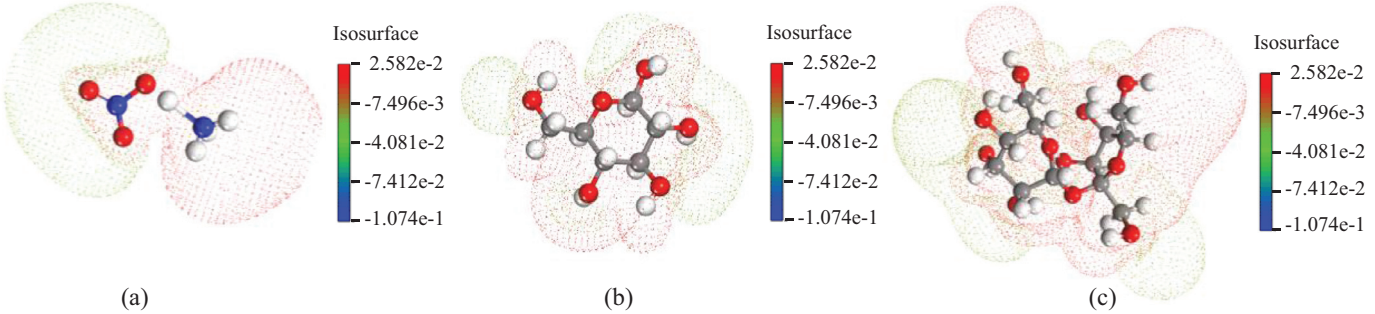

Fig. 2. Electrostatic potential maps of AN (a), glucose (b) and sucrose (c).

Table 1
Elemental carbon analyses of redox crystals of AN-GLU and AN-SU; input carbon represents the mass percent of carbon in the total solid dissolved in the solution; actual carbon denotes the measured carbon (in percentage) in the redox crystals. The carbon content for a balanced formulation (i.e., those for which OB = 0) amounts to 6.3 and 6.4% for glucose and sucrose, respectively. Input carbon is calculated from (% carbon in saccharide) × (% saccharide added to the solution)/100.

Sample	Input carbon (%)	Actual carbon (%)
AN-GLU1	0.40	0.29
AN-GLU5	2.00	0.59
AN-GLU10	4.00	0.97
AN-GLU15	6.00	1.46
AN-SU1	0.42	0.27
AN-SU5	2.1	0.61
AN-SU10	4.2	1.00
AN-SU15	6.3	1.50

(or sucrose) in 2 mL ultrapure water (resistivity 418 MΩ cm) to form a saturated solution, which was agitated in a water bath, maintained at 70 °C, for complete dissolution within 30 min. As discussed above, the concentration of the solid fuels varied from 1 to 15 wt%. The supersaturated solutions were quenched in an ice-cold water bath at 1 °C for 5 min to effect nucleation and growth of redox crystals. We filtered the solids immediately via vacuum filtration method and desiccated them in a sealable glass enclosure containing orange silica gel beads for at least 24 h before characterisation.

2.2. Material characterisation

2.2.1. Carbon content

Elemental analysis (ThermoScientific EA IsoLink Flash IRMS module) generates the percent composition of carbon in redox crystals. As indicated in Table 1, the actual amounts of carbon in the samples are lower than those employed in the sample preparation, suggesting that some saccharides remain in the solution, i.e., do not co-recrystallise proportionately with the ammonium nitrate. However, plots of the "input carbon" against "actual carbon", shown in Fig. S1 of the Supplementary Material, reveal a linear relationship, implying that, the ionic strength of AN in the solution dictates the abundance of the saccharides in the redox crystals. This type of variation stems from the synthesis route employed; the hydroxyl groups in the saccharide are stabilised by hydrogen-bonding within the interstitial positions of water molecules. The ionic strength of AN, as well as the intermolecular (weak) bonding of saccharides with water, can affect the interaction-potentials of the AN-saccharide in the system. Although we aimed to use a nonaggressive solvent (i.e., water), one can eliminate such effect by appropriate selection (e.g., based on solubility, Hildebrand value, Hansen hydrogen-bonding parameters, etc.) of cosolvent and anti-solvent [32].

2.2.2. Infrared spectroscopy

The vibrational insights from diffuse reflectance infrared Fourier transform spectroscopy (DRIFTS) elucidate the molecular interactions of glucose and sucrose in the prepared crystals. DRIFTS has been shown to be more sensitive to surface species than other solid IR sampling techniques. We employed the Agilent Cary 670 FTIR spectrometer combined with PIKE Technologies DiffusIR accessory with gold-coated optical components. The co-recrystallised samples of redox crystals were diluted at a level of 2% (w/w) in a matrix of spectroscopically pure KBr. We then transferred a thoroughly-mixed 35 mg portion of the resulting mixture into a sampling cup placed in the environmental chamber, sealed with KBr window, and, where applicable, heated up the material to the desired temperature (i.e., 200 °C at 5 °C/min) under atmosphere of inert nitrogen. The spectrometer operated at spectral resolution of 4 cm^{-1}, averaged 24 accumulated scans per spectrum, requiring the data collection time of 55 s, on a deuterated lanthanum-alanine doped triglycine sulphate (DLaTGS) detector. Figure 3 depicts the resulting IR spectra, annotating the major vibration frequencies of AN [33] and glucose [34,35]. We have recorded similar traces for the AN-SU compositions. The IR spectra of the AN-GLU redox crystals are somewhat identical to that of pure AN, except for the signatures of νCO and combination band of symmetric νCO and νCC stretches (both from glucose), as well as the broadening of the NH_4^+ peak that indicates its convolution with OH peak of glucose, i.e., a hydrogen-bond interaction between the two groups. As shown in Fig. 3(b), the νCO and νCO + νCC stretches begin to disappear at around 120 °C. This complements our observation from capillary melting-point test (Fig. S2, Supplementary Material), which indicates a colour change in the crystals (from clear white to light brown, then grey) starting at approximately 125 °C.

2.2.3. Moisture uptake

The electrostatic interaction of the saccharides with the AN changes the affinity of ammonium nitrate to moisture. Figure 4 plots and contrasts the hygroscopicity measurements of the redox crystals to that of neat ammonium nitrate, with standard errors computed from three repeated experiments. The relative humidity of 60%, typical of an extreme room condition, was achieved via standard saturated-salt-slurry (NaBr) method [36]. The moisture uptake of the redox crystals appears somewhat higher than that of pure AN after 8 h of exposure, at 24 °C. The saccharides increase the affinity of AN to moisture by 1–6%, depending on the composition of the carbohydrate. This moderate increase in hygroscopicity results in higher magnitudes of partial charges because of the formation of hydrogen bonds between the saccharides and AN.

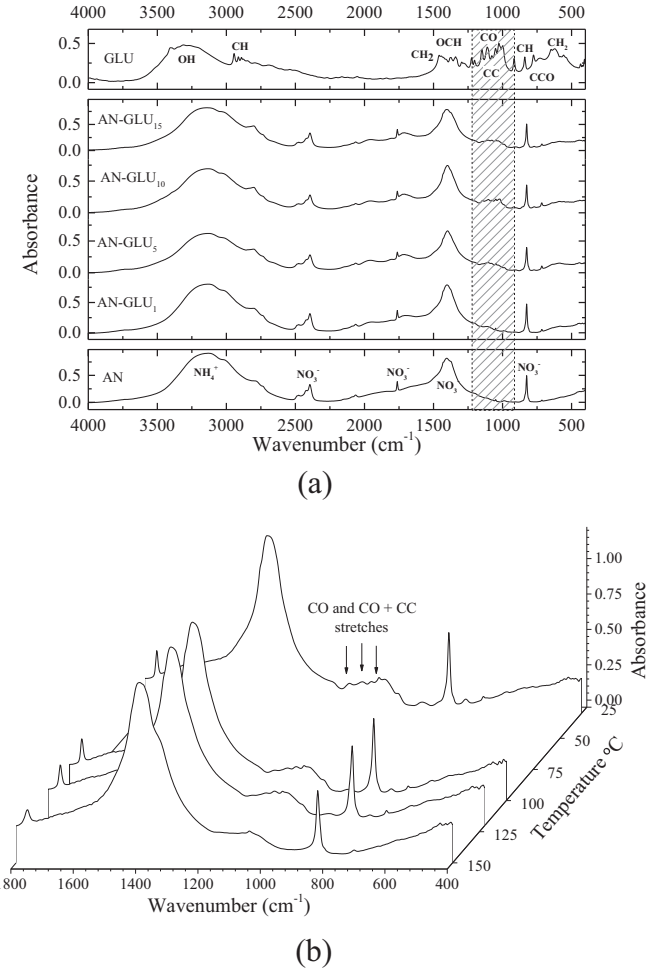

Fig. 3. DRIFTS spectra of AN-GLU formulations as compared to pure AN and glucose (a), as well as in situ temperature-based traces of AN-GLU$_{10}$ (b).

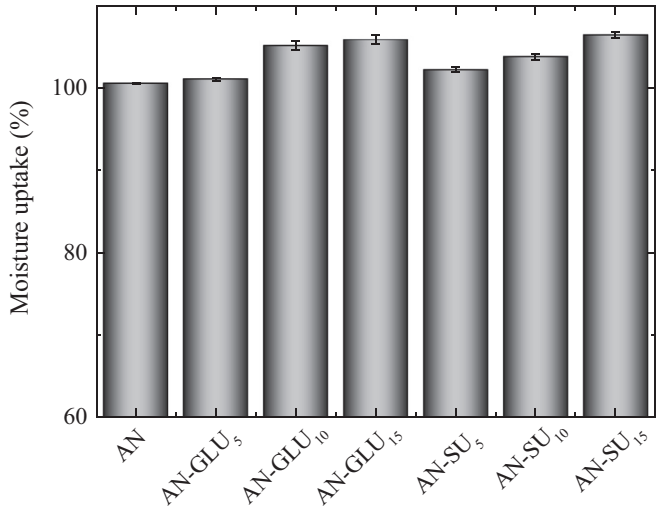

Fig. 4. Water uptake of redox crystals of AN and saccharides in air of relative humidity of 60% after 8 h, at 24 °C.

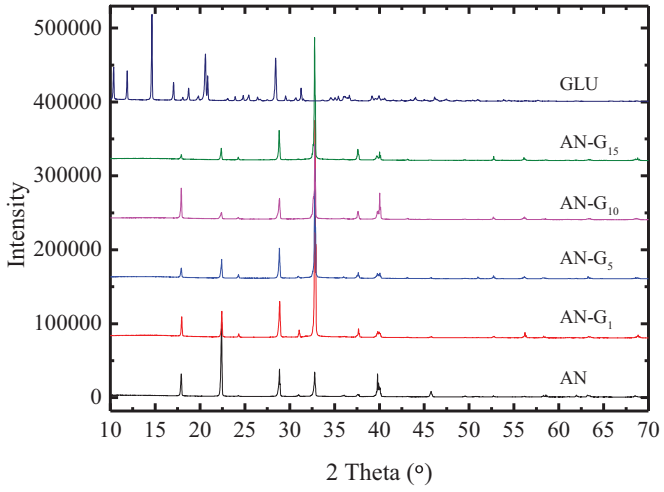

Fig. 5. Particle XRD traces of samples of AN-saccharide redox crystals.

2.2.4. Crystallographic information

The powder X-ray diffraction measurements were performed on a Panalytical Empyrean instrument using the Cu-$K\alpha_1$ radiation, operating at 40 kV and 40 mA, 1° divergence slit, with a constant step size of 0.001°. The diffractogram in Fig. 5 and DSC traces in Fig. 6 indicate that, the organic molecules do not affect the transition of phase (IV) to phase (III) of ammonium nitrate within the tested composition ratios. Golovina et al. [20] previously demonstrated that, in the case of a crystallochemical similarity of components (modifier and AN), occasionally, a large amount of an additive can be introduced into alloys without indications of the presence of this additive in the X-ray diffraction pattern. As such, the organic modifiers are distributed as fine clusters over different crystalline blocks of AN, in which the interplanar *d*-spacing adequately accommodates the additives. On this note, AN (IV) has *d*-spacings ranging from 1.3625–4.9600 Å (for different Miller indices) [37], large enough to accommodate small clusters of planar molecules of glucose and sucrose.

2.3. Thermal analysis

Simultaneous thermal analysis performed on a Netzsch STA 449 F3 Jupiter instrument served to study the thermochemical behaviour of the desiccated samples upon heating (see Fig. 6). The method employed approximately 5 mg samples, placed in an alumina crucible, and heated from 25 °C to 500 °C at the rates of 5, 10, 15 and 20 °C/min in ultra-high purity argon. The use of opened crucible eliminates the effect of secondary reactions occurring in the gas phase. These types of reactions result in the formation of AN aerosol ($NH_3 + HNO_3 \rightarrow NH_4NO_3$) [1], influencing the decomposition kinetics of AN. The continuous flow rate of the purge gases amounted to 60 mL/min, as measured under the standard temperature and pressure (STP). Blank runs completed under identical conditions to the production runs yielded the thermal buoyancy and baseline (for heat flow) corrections.

3. Results and discussion

3.1. Thermochemical analysis

Figure 6 combines the measurements of thermogravimetric analysis (TGA) with the differential scanning calorimetry (DSC). The TGA reveals that, the organic components leave little or no residue after their decomposition at 400 °C. The saccharides in the redox crystals do not result in “explosion” (usually identified as a sudden drop in mass in a TGA plot, or exothermic spike in DSC result around 150 °C), but rather display faster rates of decomposition. The heat-flow measurements (DSC) capture the change in the decomposition rate, as illustrated in the shift of the endothermic decomposition peaks. Moreover, the samples of redox

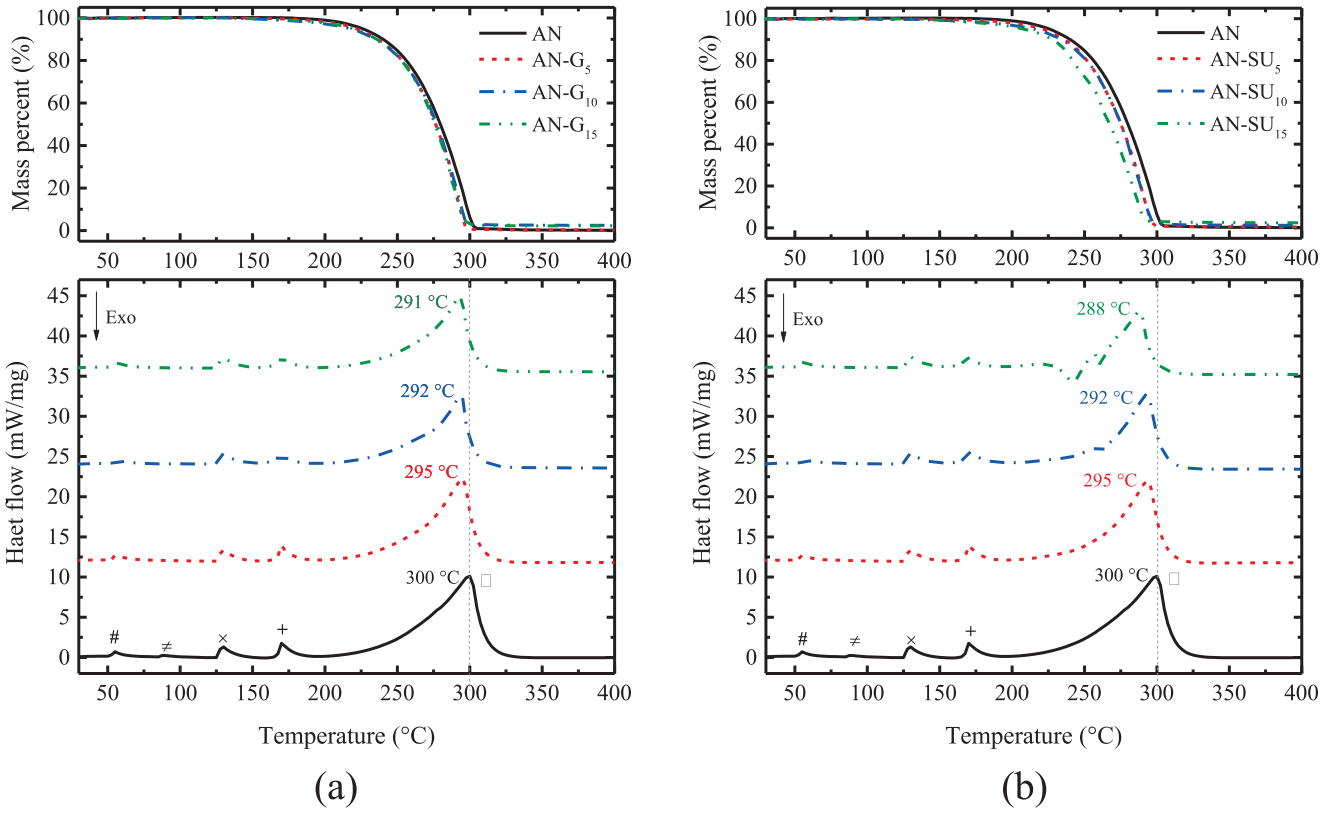

Fig. 6. TGA and DSC plots of AN-GLU (a) and AN-SU (b) samples. The symbols #, ≠, ×, +, and □ denote $AN_{IV} \rightarrow AN_{III}$, $AN_{III} \rightarrow AN_{II}$, $AN_{II} \rightarrow AN_{I}$ transitions, melting and decomposition, respectively.

crystals of AN and sucrose, prepared with 10 and 15 mass percent of sucrose incur some exothermicity likely due to the presence of reactive acetal bridges in sucrose, reducing the overall enthalpic requirement of their respective decomposition step.

Regarding the phase changes prior to decomposition, the recrystallised AN-saccharide samples do not undergo the crystalline transformation of $AN_{III} \rightarrow AN_{II}$, but rather experience a direct shift from $AN_{IV} \rightarrow AN_{II}$, as a result of lack of water trapped within the lattice structure. Humid AN generally follows IV → III → II → I (at 44 °C, 91 °C and 126 °C), while extremely dried salt of ammonium nitrate sustains the IV → II → I (at 52 °C and 126 °C) pathway [38,39]. In fact, it has been reported that, maintaining a water content below 0.01% (mass ratio) eliminates the IV → III transition, therefore phase IV transforms directly to phase II, bypassing phase III, at around 52 °C [33,40,41].

3.2. Isothermal conversion and regression rate

Figure 7 reveals better the function of the saccharide in accelerating the decomposition rate of the samples at the isothermal temperature of 250 °C. In terms of its ballistic property, pure AN has a relatively low burning rate, little affected by particle size but highly sensitive to pressure and temperature [42]. Generally, burning rate plays important roles in the case of pyrotechnic and propellant formulations, serving as indicative of their functional performance and the technological parameters for the design of the combustion ports [8]. It has been established that, the unmodified AN burns poorly under atmospheric pressure [2,43,44].

By assuming cubic samples and constant density, one can transform the decomposition rate (mg/s) of the isothermal TGA data (Fig. 7) into linear regression rate (mm/s) [45]. They are reported in Table 2. The numerical values followed from $\Delta r = \Delta v^{\frac{1}{3}} = (\frac{\Delta m}{\rho})^{\frac{1}{3}}$, hence, Rate $= \Delta r/\Delta t$. Redox crystals of AN and saccharides improve the linear regression rate of AN and should have similar impact on its high-pressure burning rate.

Table 2
Estimated regression rates for the decomposition of redox crystals of AN and saccharides.

Sample	Linear regression rate (mm/s)
AN	0.0019
AN-GLU5	0.0024
AN-GLU10	0.0027
AN-GLU15	0.0029
AN-SU5	0.0023
AN-SU10	0.0025
AN-SU15	0.0036

As shown in Fig. S3 of the Supplementary Material, the combustion mechanism of solid propellant has been partitioned into four distinctive zones, namely, the unreacted condensed phase, reacting condensed phase, gas-phase fizz, and flame zones [46–48]. Accordingly, the conductive heat feedback from the adjacent hot gaseous combustion zones drives the thermal wave (hence, the burning surface) through the regressing solid propellant [47–49]. For the case of the redox crystal samples, the conductive energy feedback instigates subsurface solid-phase reactions (involving the small quantity saccharides evenly incorporated into AN via co-recrystallisation as shown in the DRIFTS results) that enable the temperature of the solid to rise rapidly to surface temperature. This rise in temperature accelerates the thermal decomposition of propellant particles, elevating the burning rate but without causing an explosion. Moreover, energetic additives have the potential to induce exothermic reactions in the induction zone, decreasing its thickness, and hence boosting the burning rate [50]. The exothermic oxidation of the modifiers (e.g., hydrocarbon fragments

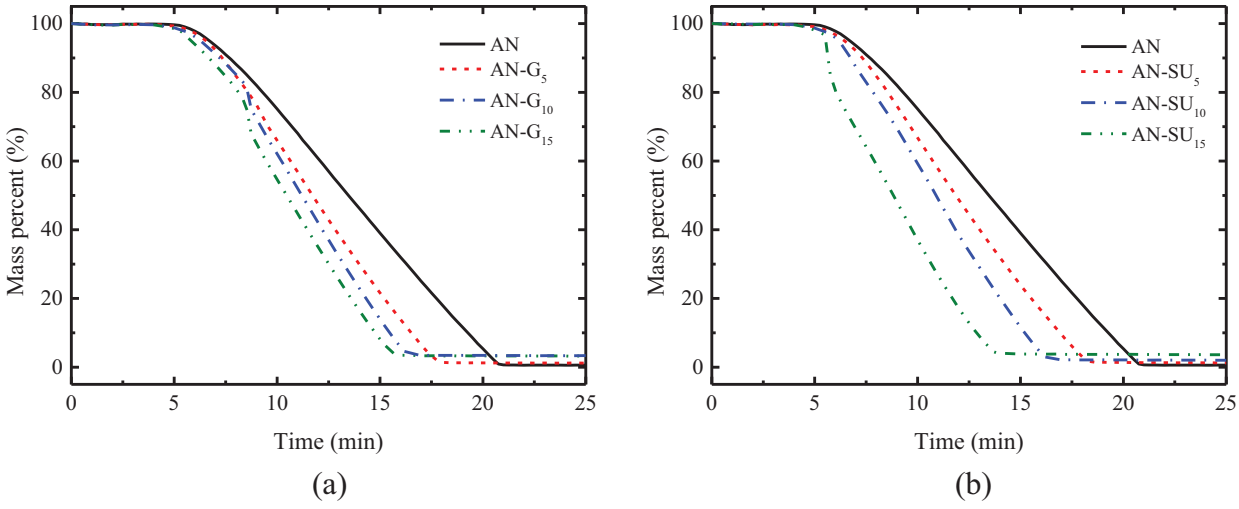

Fig. 7. Isothermal decomposition of the AN-glucose redox crystals (a) and AN-sucrose redox crystals (b) at 250 °C.

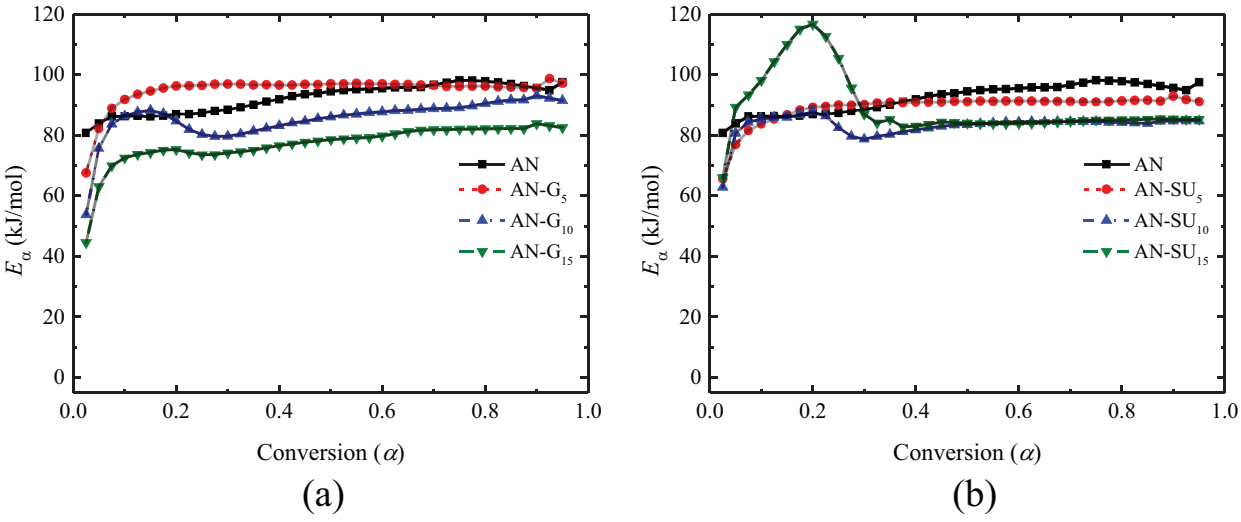

Fig. 8. Activation energies of thermal decomposition redox crystals of AN and glucose (a), and sucrose (b). The accuracy thresholds (i.e., error bars) fall inside the size of the marker symbols.

as per the saccharides) in the gas-phase can increase the combustion temperature of the induction zone, instigates hotter flames, and, as a result, intensifies the burning rate. This process also enhances the gasification of the constituents of the condensed phase.

3.3. Kinetic consideration

Advanced isoconversional method of Vyazovkin et al. [51,52] enabled an accurate estimation of activation energies for the thermal decomposition process as a function of the conversion α. Our previous study provides a detailed application of such method [53]. Briefly, for a series of runs performed at different heating rates, the activation energy (E_α, with the subscript α signifying the conversion) corresponds to a value that minimises the objective function in Eq. (2), with the integer subscripts i and j representing different experiments performed under varying heating programs, and $I(E,T)$ the Arrhenius temperature integral. We compare the results obtained from Eq. (2) with the Starink implementation of the isoconversional method [54], to examine the linearity of the kinetic functions as shown in Fig. S4, Supplementary Material.

$$\emptyset(E_\alpha) = \sum_{i=1}^{n}\sum_{j\neq i}^{n} \frac{I(E_\alpha,\ T_{\alpha,i})\beta_j}{I\left(E_\alpha, T_{\alpha,j}\right)\beta_i} \qquad (2)$$

Figure 8 plots the activation energies as a function of conversion. The E_α-dependence of pure AN amounts to 92 ± 4 kJ/mol, indicating a somewhat single-step decomposition in agreement with the previously reported range of 84 to 98 kJ/mol [55,56]. The organic modifiers (i.e., saccharides) induce changes in reaction mechanisms that manifest themselves by lowering of the activation energy, E_α, typically by 10 kJ/mol in comparison to the number for AN, as shown in Fig. 8. However, AN-SU_{15} incurs a different behaviour, where the activation energy value shoots up to 115 kJ/mol before levelling down to ca. 80 kJ/mol at $\alpha < 0.35$. Such behaviour is due to the exothermic events that are independent of high heating rates (refer to Figs. 6(b) and S5) at the onset of the thermal decomposition of AN-SU_{15}. The accelerated decomposition (with respect to pure AN), in this case, can be attributed to the relatively high entropy contribution because of larger sucrose molecules.

4. Conclusion

Co-recrystallisation of saccharides and AN (in water) does not alter the crystallographic identity of AN within the tested ratios of the modifiers. The vibrational spectroscopy elucidates the dipole–dipole interactions (i.e., the formation of hydrogen bonds) of AN with the common saccharides, facilitating an increase in the

hygroscopic nature of the samples, as compared to pure AN. Even though the elemental carbon content of the redox crystals is small, it promotes the decomposition and enhances the burning rate, as estimated by the solid regression rate. The DSC traces show that, the samples co-recrystallised with glucose do not feature exothermic transitions within the tested ratios. However, the sucrose analogue incurs exothermic decomposition, appearing for AN-SU_{15} due to a relatively high concentration of carbon and the presence of reactive acetal bridges. The kinetic analysis indicates that, the carbohydrate modifiers enhance the burning properties of AN by decreasing the activation energy of the decomposition of AN by around 10 kJ/mol. Although the new material is hygroscopic with low-temperature phase-transitions, the relatively higher regression rate should improve the burning properties of AN in propulsion activities. Furthermore, as the recrystallisation procedure brings the organic material into very close proximity with AN, such formulations (when balance with fuel oil) are expected to attenuate the formation of nitrogen oxides pollution in detonation of civilian-grade explosives.

Declaration of Competing Interest

The authors declare that they have no known competing financial interests or personal relationships that could have appeared to influence the work reported in this paper.

Acknowledgment

We are grateful to the Australian Research Council (ARC LP160101169) and Dyno Nobel Asia Pacific for funding this study. The authors acknowledge the facilities, and the scientific and technical assistance of the Australian Microscopy & Microanalysis Research Facility at the Centre for Microscopy, Characterisation & Analysis, The University of Western Australia, a facility funded by the collaborating universities as well as the State and Commonwealth Governments.

Supplementary materials

Supplementary material associated with this article can be found, in the online version, at doi:10.1016/j.combustflame.2019.11.030.

References

[1] I. Oluwoye, B.Z. Dlugogorski, J. Gore, H.C. Oskierski, M. Altarawneh, Atmospheric emission of NO_x from mining explosives: a critical review, Atmos. Environ 167 (2017) 81–96.
[2] J. Jos, S. Mathew, Ammonium nitrate as an eco-friendly oxidizer for composite solid propellants: promises and challenges, Crit. Rev. Solid State Mater. Sci. 42 (2017) 470–498.
[3] A. Ulas, G.A. Risha, K.K. Kuo, Ballistic properties and burning behaviour of an ammonium perchlorate/guanidine nitrate/sodium nitrate airbag solid propellant, Fuel 85 (2006) 1979–1986.
[4] Y.-D. Seo, S.H. Chung, J.J. Yoh, Automotive airbag inflator analysis using the measured properties of modern propellants, Fuel 90 (2011) 1395–1401.
[5] A. Grinberg Dana, G. Tvil, L. Winter, G.E. Shter, G.S. Grader, Pressure effect on the combustion of aqueous urea ammonium nitrate alternative fuel, Fuel 159 (2015) 500–507.
[6] B. Mosevitzky, G.E. Shter, G.S. Grader, Effect of equivalence ratio on the thermal autoignition of aqueous ammonia ammonium nitrate monofuel, Combust. Flame 188 (2018) 142–149.
[7] C. Oommen, S.R. Jain, Ammonium nitrate: a promising rocket propellant oxidizer, J. Hazard. Mater. 67 (1999) 253–281.
[8] J.P. Agrawal, High Energy Materials: Propellants, Explosives and Pyrotechnics, Wiley-VCH, Weinheim, 2010.
[9] Y.-I. Izato, A. Miyake, Thermal decomposition mechanism of ammonium nitrate and potassium chloride mixtures, J. Therm. Anal. Calorim. 121 (2015) 287–294.
[10] S.A. Skarlis, A. Nicolle, D. Berthout, C. Dujardin, P. Granger, Combined experimental and kinetic modeling approaches of ammonium nitrate thermal decomposition, Thermochim. Acta 584 (2014) 58–66.
[11] R. Musin, M. Lin, Novel bimolecular reactions between NH_3 and HNO_3 in the gas phase, J. Phys. Chem. A 102 (1998) 1808–1814.
[12] J. Park, M. Lin, Thermal decomposition of gaseous ammonium nitrate at low pressure: kinetic modeling of product formation and heterogeneous decomposition of nitric acid, J. Phys. Chem. A 113 (2009) 13556–13561.
[13] D. Trache, T.M. Klapötke, L. Maiz, M. Abd-Elghany, L.T. DeLuca, Recent advances in new oxidizers for solid rocket propulsion, Green Chem. 19 (2017) 4711–4736.
[14] Y.-I. Izato, A. Miyake, Detailed kinetic model for ammonium dinitramide decomposition, Combust. Flame 198 (2018) 222–229.
[15] T.M. Klapötke, Chemistry of High-Energy Materials, Walter de Gruyter GmbH & Co KG, 2017.
[16] D. Zhang, C.-Y. Cao, S. Lu, Y. Cheng, H.-P. Zhang, Experimental insight into catalytic mechanism of transition metal oxide nanoparticles on combustion of 5-Amino-1H-Tetrazole energetic propellant by multi kinetics methods and TG-FTIR-MS analysis, Fuel 245 (2019) 78–88.
[17] S. Isert, L. Xin, J. Xie, S.F. Son, The effect of decorated graphene addition on the burning rate of ammonium perchlorate composite propellants, Combust. Flame 183 (2017) 322–329.
[18] P.N. Simões, L.M. Pedroso, A.A. Portugal, J.L. Campos, Study of the decomposition of phase stabilized ammonium nitrate (PSAN) by simultaneous thermal analysis: determination of kinetic parameters, Thermochim. Acta 319 (1998) 55–65.
[19] N. Golovina, G. Nechiporenko, G. Nemtsev, G. Dolganova, V. Roshchupkin, D. Lempert, G. Manelis, Phase state stabilization of ammonium nitrate for creating an oxidizing agent for smokeless gas-generating formulations yielding no toxic combustion products, Russ. J. Appl. Chem. 80 (2007) 24–30.
[20] N. Golovina, G. Nechiporenko, G. Nemtsev, I. Zyuzin, V. Roshchupkin, D. Lempert, I. Ovchinnikov, G. Manelis, Control over phase transformations in the crystal lattice of ammonium nitrate by modification of the system of intermolecular interactions via addition of organic substances, Russ. J. Appl. Chem. 81 (2008) 1740–1746.
[21] I. Vyazenova, V. Taranushich, V. Chernyshev, V. Bogdanova, Phase stabilization of ammonium nitrate by double addition of potassium nitrate and melamine, Russ. J. Appl. Chem. 90 (2017) 1392–1396.
[22] A. Mousaviazar, M.H. Keshavarz, M. Hayaty, The effect of cellulose derivatives on the phase transition and thermal behavior of ammonium nitrate, J. Therm. Anal. Calorim. 128 (2017) 1049–1056.
[23] J.C. Oxley, J.L. Smith, E. Rogers, M. Yu, Ammonium nitrate: thermal stability and explosivity modifiers, Thermochim. Acta 384 (2002) 23–45.
[24] A. Nazarian, C. Presser, Thermal signature measurements for ammonium nitrate/fuel mixtures by laser heating, Thermochim. Acta 623 (2016) 120–135.
[25] S.A. Resende, H.M.D. Lima, Study of non-conventional fuels for explosives mixes, Rem: Revista Escola de Minas 67 (2014) 297–302.
[26] R. Yang, P. Thakre, Y.-C. Liau, V. Yang, Formation of dark zone and its temperature plateau in solid-propellant flames: a review, Combust. Flame 145 (2006) 38–58.
[27] B. Delley, An all-electron numerical method for solving the local density functional for polyatomic molecules, J. Chem. Phys. 92 (1990) 508–517.
[28] B. Delley, From molecules to solids with the $DMol^3$ approach, J. Chem. Phys. 113 (2000) 7756–7764.
[29] A. Tkatchenko, M. Scheffler, Accurate molecular van der Waals interactions from ground-state electron density and free-atom reference data, Phys. Rev. Lett. 102 (2009) 073005.
[30] D. Xiang, W. Zhu, H. Xiao, Thermal decomposition mechanisms of energetic ionic crystal dihydrazinium 3,3′-dinitro-5,5′-bis-1,2,4-triazole-1,1-diolate: an ab initio molecular dynamics study, Fuel 202 (2017) 246–259.
[31] P.W. Cooper, Explosives Engineering, Wiley-Vch, 1996.
[32] T. Lee, J.W. Chen, H.L. Lee, T.Y. Lin, Y.C. Tsai, S.-L. Cheng, S.-W. Lee, J.-C. Hu, L.-T. Chen, Stabilization and spheroidization of ammonium nitrate: co-crystallization with crown ethers and spherical crystallization by solvent screening, Chem. Eng. J. 225 (2013) 809–817.
[33] H.B. Wu, M.N. Chan, C.K. Chan, FTIR characterization of polymorphic transformation of ammonium nitrate, Aerosol Sci. Technol. 41 (2007) 581–588.
[34] M. Ibrahim, M. Alaam, H. El-Haes, A.F. Jalbout, A.D. Leon, Analysis of the structure and vibrational spectra of glucose and fructose, Eclética Quim. J. 31 (2006) 15–21.
[35] G. Dai, K. Wang, G. Wang, S. Wang, Initial pyrolysis mechanism of cellulose revealed by in-situ drift analysis and theoretical calculation, Combust. Flame 208 (2019) 273–280.
[36] A. Standard, A.S.T.M. E104-02, Standard Practice for Maintaining Constant Relative Humidity by Means of Aqueous Solutions, American Society for Testing Materials, Philadelphia, 2002.
[37] S.B. Hendricks, E. Posnjak, F.C. Kracek, Molecular rotation in the solid state. the variation of the crystal structure of ammonium nitrate with temperature, J. Am. Chem. Soc. 54 (1932) 2766–2786.
[38] M.J. Herrmann, W. Engel, Phase transitions and lattice dynamics of ammonium nitrate, Propellants Explos. Pyrotech. 22 (1997) 143–147.
[39] C.N.R. Rao, M. Natarajan, B. Prakash, Crystal Structure Transformations in Inorganic Nitrites, Nitrates, and Carbonates, National Bureau of Standards, United StatesWashington, 1975.
[40] C. Sjölin, Influence of moisture on the structure and quality of ammonium nitrate prills, J. Agric. Food. Chem. 19 (1971) 83–95.
[41] C. Sjölin, Mechanism of caking of ammonium nitrate (NH_4NO_3) prills, J. Agric. Food. Chem. 20 (1972) 895–900.

[42] L. De Luca, L. Galfetti, F. Severini, M. Galeotta, R. De Amicis, V. Babuk, B. Kondrikov, A. Vorozhtsov, Low-Cost and green solid propellants for space propulsion, in: A. Wilson (Ed.), 2nd International Conference on Green Propellants for Space Propulsion (ESA SP-557), Sardinia, Italy, ESA Special Publication (2004).
[43] M. Beckstead, Burn Rate Mechanisms. Volume 2. A Model for Ammonium Nitrate Propellant Combustion, Brigham Young University Department Of Chemical Engineering, and Astronautics Laboratory-Air Force Space Technology Center, CA, 1990.
[44] W. Andersen, K. Bills, E. Mishuck, G. Moe, R. Schultz, A model describing combustion of solid composite propellants containing ammonium nitrate, Combust. Flame 3 (1959) 301–317.
[45] N. Gascoin, G. Fau, P. Gillard, A. Mangeot, Experimental flash pyrolysis of high density polyethylene under hybrid propulsion conditions, J. Anal. Appl. Pyrolysis 101 (2013) 45–52.
[46] Y.I. Izato, A. Miyake, S. Date, Combustion characteristics of ammonium nitrate and carbon mixtures based on a thermal decomposition mechanism, Propellants, Explosives, Pyrotechnics 38 (2013) 129–135.
[47] C. Dennis, B. Bojko, On the combustion of heterogeneous ap/htpb composite propellants: a review, Fuel 254 (2019) 115646.
[48] D. Zhang, S. Lu, C.-Y. Cao, C.-C. Liu, L.-L. Gong, H.-P. Zhang, Impacts on combustion behavior of adding nanosized metal oxide to CH_3N_5-$Sr(NO_3)_2$ propellant, Fuel 191 (2017) 371–382.
[49] M. Kohga, S. Togo, Influence of iron oxide on thermal decomposition behavior and burning characteristics of ammonium nitrate/ammonium perchlorate-based composite propellants, Combust. Flame 192 (2018) 10–24.
[50] S. Elbasuney, A. Fahd, H.E. Mostafa, Combustion characteristics of extruded double base propellant based on ammonium perchlorate/aluminum binary mixture, Fuel 208 (2017) 296–304.
[51] S. Vyazovkin, Advanced isoconversional method, J. Therm. Anal. 49 (1997) 1493–1499.
[52] S. Vyazovkin, A.K. Burnham, J.M. Criado, L.A. Pérez-Maqueda, C. Popescu, N. Sbirrazzuoli, ICTAC kinetics committee recommendations for performing kinetic computations on thermal analysis data, Thermochim. Acta 520 (2011) 1–19.
[53] I. Oluwoye, B.Z. Dlugogorski, J. Gore, S. Vyazovkin, O. Boyron, M. Altarawneh, Thermal reduction of NO_x with recycled plastics, Environ. Sci. Technol. 51 (2017) 7714–7722.
[54] M.J. Starink, The determination of activation energy from linear heating rate experiments: a comparison of the accuracy of isoconversion methods, Thermochim. Acta 404 (2003) 163–176.
[55] S. Vyazovkin, J.S. Clawson, C.A. Wight, Thermal dissociation kinetics of solid and liquid ammonium nitrate, Chem. Mater. 13 (2001) 960–966.
[56] T. Liavitskaya, N. Guigo, N. Sbirrazzuoli, S. Vyazovkin, Further insights into the kinetics of thermal decomposition during continuous cooling, PCCP 19 (2017) 18836–18844.